Planetary and Space Science 113-114 (2015) 309–320

Contents lists available at ScienceDirect

Planetary and Space Science

journal homepage: www.elsevier.com/locate/pss

Update of the Venus density and temperature profiles at high altitude measured by SOIR on board Venus Express

A. Mahieux [a,b,c,*], A.C. Vandaele [a], S.W. Bougher [d], R. Drummond [a], S. Robert [a], V. Wilquet [a], S Chamberlain [a], A. Piccialli [e], F. Montmessin [e], S. Tellmann [f], M. Pätzold [f], B. Häusler [g], J.L. Bertaux [e,h]

[a] Planetary Aeronomy, Belgian Institute for Space Aeronomy, 3 av. Circulaire, B-1180 Brussels, Belgium
[b] Fonds National de la Recherche Scientifique, rue d'Egmont 5, B-1000 Brussels, Belgium
[c] Department of Planetary Sciences, University of Arizona, 1629 E. University Blvd, Tucson, AZ 85721, United States
[d] Department of Atmospheric, Oceanic, and Space Sciences, University of Michigan, 2455 Hayward St., Ann Arbor, MI 48109, United States
[e] LATMOS—UVSQ/CNRS/IPSL, 11 bd d'Alembert, 78280 Guyancourt, France
[f] Abteilung Planetenforschung, Rheinisches Institut für Umweltforschung, Universität zu Köln, Cologne, Germany
[g] Institut für Raumfahrttechnik, Universität der Bundeswehr München, Neubiberg, Germany
[h] Institut Pierre Simon Laplace, Université de Versailles-Saint-Quentin, 78280 Guyancourt, France

ARTICLE INFO

Article history:
Received 27 February 2014
Received in revised form
19 August 2014
Accepted 2 February 2015
Available online 13 February 2015

Keywords:
Planetary atmosphere
Venus
Temperature

ABSTRACT

The SOIR instrument on board Venus Express regularly sounds the Venus atmosphere using the solar occultation technique. The density and temperature profiles are inferred from SOIR spectra recorded in the infrared. The method has been described in a previous publication (Mahieux et al., 2012. J. Geophys. Res. 117. doi:10.1029/2012JE004058.). This paper is devoted to the update of the VAST (Venus Atmosphere from SOIR measurements at the Terminator) compilation that was initiated in the above cited work, which gives the mean CO_2 number density and temperature profiles for different latitude bins. The method has been improved and has been applied to more data. The new compilation which is given on the same latitudinal grid now distinguishes between the two sides of the terminator. The compilation also confirms the main thermal layering characteristics that were identified in the earlier version: the succession of a warm layer (230 ± 30 K, $1-\sigma$ standard deviation) at a pressure level of 3.2×10^{-7} mbar ($\sim$140 km), a very cold layer (125 ± 32 K) at 2.5×10^{-5} mbar ($\sim$123 km), a warm layer (204 ± 17 K) at 0.01 mbar ($\sim$102 km) and finally a colder layer at 0.4 mbar (171 ± 34 K, $\sim$87 km). The layering of all the temperature profiles is explained by radiative rather than dynamical processes. The temporal temperature variation is larger than the mean latitudinal temperature variation. VAST is compared with temperature profiles obtained from other Venus Express instruments, VeRa and SPICAV–UV, and ground based measurements.

1. Introduction

This paper is dedicated to the description of the Venus terminator in terms of number densities and temperature, focusing on the mesosphere (70 to 95 km) and lower thermosphere (95 to 150 km) regions. These are poorly known regions of the Venus atmosphere. Few measurements of the region have been published so far, either concentrating on a narrow region, for example at an approximate altitude of 110 km and covering all latitudes (Sonnabend et al., 2012), or deriving vertical profiles at a single latitude at the terminator, such as in Seiff et al. (1980). Most of the previous measurements focus on the mesosphere and cloud layer regions, either on the day or night sides (Clancy et al., 2008, 2012; Grassi et al., 2010; Migliorini et al., 2012; Stewart, 1968; Tellmann et al., 2012, 2009; Zasova et al., 1996). Piccialli et al. (2015) obtained night time profiles between 90 and 130 km from SPICAV–UV on board Venus Express (VEx) using stellar occultation. Information about the Venus terminator is accessible through global computation models, and is compared for the first time to real measurements of density and temperature profiles (Bougher et al., 2015), obtained from the SOIR instrument, and helps understand the local energy balance at the terminator.

The Solar Occultation in the InfraRed (SOIR) instrument on board the Venus Express spacecraft is a spectrometer dedicated to the study of the Venus terminator (Bertaux et al., 2007), which performs daily observations of the 70–170 km altitude region, at latitudes

* Corresponding author at: Planetary Aeronomy, Belgian Institute for Space Aeronomy, 3 av. Circulaire, B-1180 Brussels, Belgium.
E-mail address: arnaud.mahieux@aeronomie.be (A. Mahieux).

http://dx.doi.org/10.1016/j.pss.2015.02.002
0032-0633/

extending from Pole to Pole. It is sensitive to several key Venus species, including carbon dioxide, the main atmospheric constituent below the homopause and up to around an altitude of 150 km. Other compounds such as CO (Vandaele et al., 2015), HCl and HF (Mahieux et al., 2015b), H_2O and HDO (Fedorova et al., 2008) and SO_2 (Belyaev et al., 2012; Mahieux et al., 2015a) are also detected. Information about the aerosol composition below 90 km is furthermore derived from the SOIR measurements (Wilquet et al., 2012, 2009). Temperature profiles can be deduced with good precision from the CO_2 densities using the hydrostatic equation (Mahieux et al., 2010, 2012) and results of an independent study of the temperature profiles, which are directly derived from the rotational structure of the CO_2 observed bands, presented in the companion paper Mahieux et al. (2015b), confirm the structure of the hydrostatic temperature profiles.

This work is an update of the previously published results from the SOIR instrument about CO_2 density and temperature profiles (Mahieux et al., 2012), from which a Venus Atmosphere from SOIR data at the Terminator (VAST) compilation was obtained for different latitude bins. This paper describes in detail the improvements that were implemented into the retrieval algorithm, as well as the larger dataset on which the latest VAST compilation is built. We also compare VAST results with those from SPICAV–UV and VeRa experiments on VEx, to previous measurements obtained using Pioneer Venus and to some ground-based measurements.

2. Instrument description

SOIR, one of the instruments on board the ESA VEx mission, has been sounding the Venus atmosphere since June 2006. The instrument characteristics and measurement principles have been described in Mahieux et al. (2008, 2009), Nevejans et al. (2006) and Vandaele et al. (2013). A short summary is given here.

The instrument is sensitive in the near-infrared (NIR, 2.29 to 4.43 μm or 2257 to 4430 cm^{-1}). It uses an echelle grating as diffracting element which works at very high diffraction orders (numbered 101 to 194). An Acousto Optical Tunable Filter (AOTF) is used to select the appropriate diffraction order. The spectra are measured at a high spectral resolution provided with a summary of the main instrument characteristics in Table 1.

The SOIR spectra need careful interpretation. The AOTF transfer function was designed to have its full width at half maximum (FWHM) equal to the echelle free spectral range (21 cm^{-1}); however, during flight it was measured to be ~24 cm^{-1} (Mahieux et al., 2008). This results in spectral leakage from the adjacent orders such that absorption lines from the first adjacent orders are also present in the recorded spectra. Usually three orders either side of the selected order need to be considered to correctly account for the presence of all the structures seen in one recorded spectrum.

SOIR measures up to four diffraction orders during each occultation. Each order is measured every second (with a maximum integration time of 250 ms per order). The detector has two bins in its spatial direction; therefore, eight spectra are recorded per second by the instrument. The instrument slit is a 2′ (spatial direction) by 30′ (spectral direction) rectangle. During a solar occultation, the spacecraft is set to inertial mode and its attitude is such that the large side of the slit remains almost parallel to the limb. It is exactly parallel at a tangent altitude of 120 km. As a consequence, small tilting angles are observed at other altitudes (usually less than 5°). An altitude is assigned to the observation (Vandaele et al., 2013), corresponding to the central part of the slit (called bin hereafter). Refraction is not taken into account in the tangent altitude calculation, because it does not play any significant role above 70 km at SOIR wavelengths; transmittances measured below 70 km have too low signal, usually lower than 0.2.

Table 1
Main SOIR instrument characteristics. Details are provided for three different CO_2 orders.

Instrument characteristics	Order 112	Order 148	Order 166
Centre of the order [cm^{-1}]	2513.7	3321.5	3725.7
Spectral interval on the detector [cm^{-1}]	21.5	28.4	31.9
Spectral resolution [cm^{-1}]	0.121	0.158	0.176
Spectral sampling interval [cm^{-1}]	0.065	0.089	0.097
Typical signal to noise ratio	1500	3000	2200

Due to the elliptical orbit of the VEx spacecraft, the vertical resolution of the instrument (the vertical altitude range sounded by the projected slit at the limb in the atmosphere during the time of a measurement, see Vandaele et al. (2008)) is best at the North Pole (200 m) and degrades towards the South Pole (up to 5 km), while the vertical sampling (the vertical distance between the mean altitude of two successive soundings) is best at 45°N (500 m) and degrades towards the North Pole to 2 km and to 5 km at the South Pole. Because of the measurement technique, all the observations are made at either at 6.00 AM or 6.00 PM (Mahieux et al., 2008; Vandaele et al., 2013) and cover all latitudes.

3. Method description

The algorithm used to inverse the spectra measured by the SOIR instrument, ASIMAT, has been presented in Mahieux et al. (2010, 2012), Vandaele et al. (2015) and its principles will be summarized here. In particular, the improvements to the code will be described and discussed.

ASIMAT is an iterative algorithm working in two steps. In a first step, each of the eight spectral sets are inverted using a forward model implemented in the Bayesian method developed by Rodgers (2000), in an onion peeling frame (see Mahieux et al., 2010 for more details). Only the measurements that contain spectral signatures are considered. A dedicated routine deals with this part, considering the first spectrum as the one in which an absorption signature is first observed above the noise; the last spectrum is the one just before atmospheric saturation appears for the strongest ro-vibrational line of the weakest vibrational band simulated (Mahieux et al., 2010). The algorithm fits the logarithm of the number density of the different absorbing species and the spectral baseline. The baseline, which is related to the absorption by atmospheric aerosols (Wilquet et al., 2009) is modeled by a fifth order polynomial. The atmospheric temperature profile is not fitted at this stage.

In a second step the density profiles derived for each molecular species from each spectral set are combined into one single profile defined on a 1 km step scale using a moving average algorithm. This moving average performs a weighted linear fit of all available individual density values corresponding to altitudes located within a plus or minus two scale height region. The weights are taken as the inverse of the uncertainties on the individual number densities obtained in the first step, from the Rodgers algorithm. If carbon dioxide is among the fitted species, a temperature profile is derived from the CO_2 density vertical profile using the hydrostatic equilibrium equation. Two cases have to be considered: the homosphere and the heterosphere regions, where the use of this law slightly changes. In the homosphere region, where all the species are supposed to be well mixed, the hydrostatic equilibrium is calculated considering the total mass density profile. The CO_2 volume mixing ratio (VMR) and total molar mass profiles are taken from the Venus International Reference Atmosphere (VIRA taken from Hedin et al., 1983; Zasova et al., 2007). In the heterosphere, each species follows its own scale height: the CO_2 number density profile only is considered, and no hypothesis needs to be made on the atmospheric composition.

It is known that the homopause is not localized at a precise altitude, but corresponds to a transition region between the larger influence of the eddy diffusion and the molecular diffusion (Banks and Kockarts, 1973). In this work, we make the assumption that the transition occurs at a precise altitude level, calculated as in von Zahn et al. (1980) and corresponding approximatively to a pressure level of 10^{-6} mbar (approximatively 135 km). The error in the temperature profile introduced by this simplification remains small, since CO_2 is still the main atmospheric constituent at this pressure level (the VIRA CO_2 VMR is equal to 85% at 132 km). Tests have been run, considering altitude variations of the homopause level, and confirm this (Mahieux et al., 2012). The boundary condition for deriving the temperature is taken at the top of the profile from the previous VAST model. Dependence on this boundary condition is observed down to one scale height below the upper boundary. To determine the uncertainty on the temperature profile, CO_2 number density profiles are randomly generated within the sigma limits of the derived CO_2 vertical density profile ($=CO_2$ retrieved value + uncertainty on the CO_2 density $\times$ random vector varying between -1 and 1) and the temperature profile is determined for every case. Typically 100 random profiles are generated and the standard deviation at each level of these temperature profiles is taken as the uncertainty on the retrieved temperature profile.

ASIMAT iterates on these two steps, taking the number density and temperature profiles obtained from the second step of the previous iteration as a-priori for the Bayesian algorithm. Convergence occurs when the number density and the temperature profiles are all within the uncertainty of the previous step, and reciprocally (Mahieux et al., 2012), which usually occurs after three to four iterations. Finally, the outputs provided by the algorithm are profiles of the number densities of each individual gas, the temperature, the total number density and the pressure, with their associated errors.

Modifications relative to the previous VAST compilation concern two aspects: (1) new calibration and instrument characterization have been performed since then, see Vandaele et al. (2013); (2) improvements have been made to the algorithm since the last published version (Mahieux et al., 2012), and are described here.

The main algorithm improvement has been implemented in the ray tracing procedure. In the previous version, the ray tracing was calculated by considering only one light path corresponding to a line of sight (LOS) defined between the tangent height and the center of the selected bin on the slit. Since the vertical resolution of the instrument is varying greatly with the latitude of the measurement, this introduced a bias in the retrieval. This was seen in the results as an altitude shift with latitude. To solve this issue, a multi ray tracing calculation has been introduced in the inversion procedure. In the improved algorithm, 24 light paths spread on the slit in both directions are now considered, see Fig. 1, and the measurement at one altitude level is calculated as the algebraic average of the contributions of all paths. This improvement slightly modifies the density profiles. In fact, the shape of the profiles is not changed but the altitudes at which the minima and maxima occur are shifted to lower altitudes. This effect is more pronounced for Southern observations: the measurements taken at latitudes lower than 60°N are the most affected, because the vertical resolution becomes larger than the vertical sampling. As a result, the Northern–Southern asymmetry that was observed in Mahieux et al. (2012) version has now disappeared.

Another improvement of the algorithm concerns the correction of a caveat introduced by the Bayesian algorithm in the iterative retrieval process described above. To limit the dependence of the fitted number density profiles to the a-priori profiles, only the number density values that were fitted for each profile are taken into account. This number is given by the degree of freedom (DOF) of the retrieval extracted from the averaging kernel matrix. The DOF indicates the total number of independent pieces of information that can be derived from the observations.

Fig. 1. Left: geometric position (cross) in the slit (depicted as the box) of the point used for the ray tracing calculation in the previous configuration. Right: position of the points used for the multi ray tracing in the slit used in the new configuration.

4. Results

4.1. Database description

Since Mahieux et al. (2012), more observations were performed and analyzed. As in the previous paper, only orbits in which CO_2 is observed at high altitudes are considered, i.e. orbits during which orders between 156 and 166 were measured. The old dataset contained 59 observations; many new observations have been obtained since then: the new dataset contains 122 occultations, of which 60 are dusk observations, and 62 at dawn. All the previous measurements have been reanalyzed using the updated algorithm. The updated list of the studied orbits is given in Table 2, together with details on the measurement location, such as the VEx occultation season (OS), the Earth date, the longitude and latitude, and the local solar time (LST). The list of the vibrational bands absorbing in the different orders can be found in Mahieux et al. (2012).

The location of the measurements is presented in Fig. 2, the orbit number as a function of the latitude. The local solar time is always equal to 6.00 AM, represented by triangles in Fig. 2, or 6.00 PM, represented as circles.

4.2. CO_2 number density profiles

The CO_2 number density profiles for all orbits of Table 2 are presented in Panel A of Fig. 3. The error bars are not shown for the sake of clarity. In function of altitude, the mean error on the CO_2 number density varies between 20% at 160 km, 6% at 145 km, 35% at 120 km and 5% at 75 km—the average value for all altitudes is 14%. In the plot, the color code indicates the absolute latitude: blue shades for equatorial observations and red shades for polar observations, see also Fig. 2. The profiles are plotted as a function of the altitude, and present large variations at a given altitude level. We calculate the weighted geometric standard deviation factor, which is the standard deviation of an exponential variable. This factor for the CO_2 number density vertical profile varies between 2 and 4 in the 70–115 km region and above 135 km to a maximum of 7 in the 115–135 km region; its average value on the whole profile is equal to 3. This means that when considering all altitudes together the retrieved profiles are within the range defined by the average profile /3 and the average profile $\times 3$. The variability observed can also be discussed in terms of altitude variations for a given number density value. The standard deviation averaged on the whole profile is equal to 3.3 km, increasing from 2 km for the largest densities to 4 km for the lowest ones.

Table 2
List of the orbits studied in this work; the orbit number, VEx occultation season number, Earth date [DD/MM/YY], longitude [degree], latitude [degree] and local solar time (LT [hour]) are given.

Orbit	OS	D/MM/YYYY	Lon	Lat	LT
35.1	1	26/05/06	304	74	6
335.1	4	22/03/07	319	−16	18
361.1	4	17/04/07	208	79	6
593.1	6	05/12/07	215	3	6
597.1	6	09/12/07	226	37	6
667.1	7	17/02/08	259	78	18
669.1	7	19/02/08	263	79	18
671.1	7	21/02/08	268	81	18
674.1	7	24/02/08	273	83	18
675.1	7	25/02/08	275	83	18
677.1	7	27/02/08	277	84	18
679.1	7	29/02/08	277	85	18
681.1	7	02/03/08	274	86	18
684.1	7	05/03/08	257	88	18
685.1	7	06/03/08	247	88	18
686.1	7	07/03/08	235	88	18
687.1	7	08/03/08	223	88	6
688.1	7	09/03/08	213	87	6
689.1	7	10/03/08	205	87	6
690.1	7	11/03/08	200	87	6
691.1	7	12/03/08	197	86	6
693.1	7	14/03/08	194	85	6
695.1	7	16/03/08	194	84	6
697.1	7	18/03/08	196	82	6
699.1	7	20/03/08	198	81	6
703.1	7	24/03/08	206	77	6
705.1	7	26/03/08	210	74	6
706.1	7	27/03/08	212	73	6
709.1	7	30/03/08	219	67	6
710.1	7	31/03/08	221	63	6
710.2	7	31/03/08	217	21	6
711.1	7	01/04/08	223	58	6
1121.1	11	16/05/09	214	81	18
1124.1	11	19/05/09	234	−44	18
1125.1	11	20/05/09	220	84	18
1126.1	11	21/05/09	240	−52	18
1128.1	11	23/05/09	247	−60	18
1130.1	11	25/05/09	255	−69	18
1132.1	11	27/05/09	264	−77	18
1137.1	11	01/06/09	161	88	6
1139.1	11	03/06/09	91	−75	6
1141.1	11	05/06/09	100	−67	6
1154.1	11	18/06/09	144	−7	6
1252.1	12	24/09/09	95	−73	6
1254.1	12	26/09/09	98	−65	6
1256.1	12	28/09/09	103	−57	6
1258.1	12	30/09/09	108	−48	6
1381.2	13	31/01/10	126	16	6
1461.1	14	21/04/10	203	84	18
1462.1	14	22/04/10	192	−47	18
1464.1	14	24/04/10	219	86	18
1465.1	14	25/04/10	200	−60	18
1467.1	14	27/04/10	242	87	18
1469.1	14	29/04/10	207	−76	18
1480.1	14	10/05/10	37	86	6
1565.1	15	03/08/10	150	72	18
1567.1	15	05/08/10	159	−10	18
1581.1	15	19/08/10	159	87	18
1697.1	16	13/12/10	117	−88	18
1789.1	17	15/03/11	123	11	18
1798.1	17	24/03/11	141	81	18
1802.1	17	28/03/11	145	84	18
1804.1	17	30/03/11	144	85	18
1807.1	17	02/04/11	191	−82	18
1895.2	18	29/06/11	89	65	18
1902.1	18	06/07/11	114	79	18
1904.1	18	08/07/11	122	81	18
1910.1	18	14/07/11	148	85	18
1914.1	18	18/07/11	173	87	18
2153.1	20	13/03/12	303	87	6
2159.1	20	19/03/12	335	85	6
2238.1	21	06/06/12	67	43	18
2254.1	21	22/06/12	122	−71	18
2258.1	21	26/06/12	215	−88	18

Table 2 (*continued*)

Orbit	OS	D/MM/YYYY	Lon	Lat	LT
2272.1	21	10/07/12	351	−18	6
2273.1	21	11/07/12	355	−11	6
2274.1	21	12/07/12	358	−4	6
2275.1	21	13/07/12	1	3	6
2276.1	21	14/07/12	5	12	6
2343.2	22	19/09/12	30	65	18
2351.1	22	27/09/12	54	−14	18
2353.1	22	29/09/12	60	−23	18
2355.1	22	01/10/12	66	−31	18
2357.1	22	03/10/12	72	−39	18
2359.1	22	05/10/12	78	−47	18
2361.1	22	07/10/12	83	−55	18
2362.1	22	08/10/12	108	86	18
2363.1	22	09/10/12	88	−62	18
2366.1	22	12/10/12	141	88	18
2368.1	22	14/10/12	166	88	18
2370.1	22	16/10/12	73	−87	18
2372.1	22	18/10/12	326	−85	6
2376.1	22	22/10/12	264	87	6
2380.1	22	26/10/12	289	86	6
2386.1	22	01/11/12	345	−34	6
2388.1	22	03/11/12	326	84	6
2392.1	22	07/11/12	342	83	6
2396.1	22	11/11/12	14	8	6
2396.2	22	11/11/12	357	82	6
2401.1	22	16/11/12	29	32	6
2401.2	22	16/11/12	17	79	6
2404.1	22	19/11/12	37	47	6
2404.2	22	19/11/12	29	77	6
2463.1	23	17/01/13	41	48	18
2464.1	23	18/01/13	43	57	18
2468.1	23	22/01/13	57	−13	18
2469.1	23	23/01/13	61	−19	18
2472.1	23	26/01/13	71	−37	18
2481.1	23	04/02/13	111	−83	18
2483.1	23	06/02/13	249	−87	6
2485.1	23	08/02/13	281	−77	6
2487.1	23	10/02/13	291	−67	6
2494.1	23	17/02/13	316	−29	6
2496.1	23	19/02/13	323	−17	6
2498.1	23	21/02/13	329	−3	6
2499.1	23	22/02/13	333	5	6
2500.1	23	23/02/13	336	15	6
2570.1	24	04/05/13	11	72	18
2577.1	24	11/05/13	36	80	18
2621.1	24	24/06/13	333	81	6
2625.1	24	28/06/13	348	79	6
2629.1	24	02/07/13	11	43	6

The density profiles are all characterized by a systematic change of slope in the 110–140 km region. The large variation of the CO_2 number density is striking, even more so at lower altitudes, where smaller variations are expected. However, we attribute these variations to different effects. First of all, the measurements are taken across the terminator, i.e. half of the absorption line path of each measurement is located on the night side, and half on the day side, with large density and temperature differences on each side for a given altitude level (Bougher et al., 2015). The shape of the density and temperature gradient between night and day sides are largely unknown, as are any possible temporal variations: it does however influence the retrieved density profiles. Second, the Venus atmosphere is known to be highly variable, which is also observed by other instruments, such as SPICAV–UV/VEx (Piccialli et al., 2015), and the drag observations performed during the aerobraking phase of VEx (Svedhem, 2014).

4.3. Temperature profiles

The corresponding temperature profiles are plotted in Panel B of Fig. 3 with the same color code as in Panel A. The temperature profiles are plotted as a function of the total pressure to remove the observed density variations measured at a given altitude level. The error bars are not shown for the sake of clarity. Their mean value varies between 7 and 15 K below 110 km and between 12 and 50 K at higher altitude, with an average value on the whole pressure range equal to 19 K. The weighted standard deviation calculated on all the temperature profiles varies between 20 and 30 K above 10^{-7} mbar (143 km) and between 30 and 55 K below. The average value considering the whole pressure range is 39 K. The errors on the temperature profiles are smaller than the variability from orbit to orbit, which indicates that the variability is not induced by the uncertainty on the temperature profiles.

The CO_2 number density change of slope in the 110–140 km region is reflected in the temperature profiles as the succession of the warm and cold, whose positions do not vary much from one profile to the other. A mean temperature profile is derived from all the profiles presented in Fig. 3, and indicates the presence of a warm region at 6.3 mbar (approximately 75 km, bottom of the profile) with a mean maximum value of 216 K $\pm$ 23 K ($1-\sigma$ standard deviation of all profiles at that pressure level), on top of which a cold layer is found at the 0.4 mbar pressure level (approximately 87 km) with a

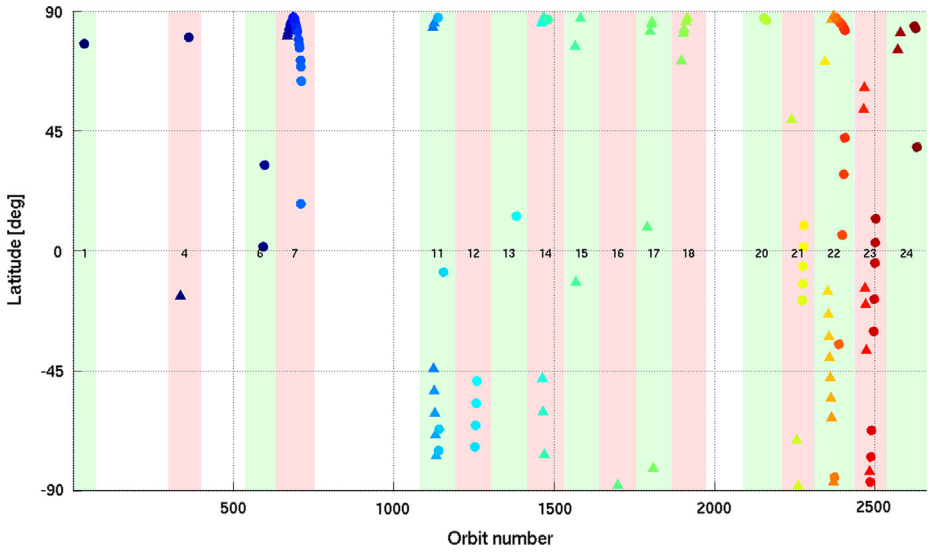

Fig. 2. Location of the measurements listed in Table 2, in terms of orbit number versus latitude of the observations. The color code is the absolute latitude, circles are morning measurements and triangles are evening measurements. The occultation season number is also indicated. (For interpretation of the references to color in this figure legend, the reader is referred to the web version of this article.)

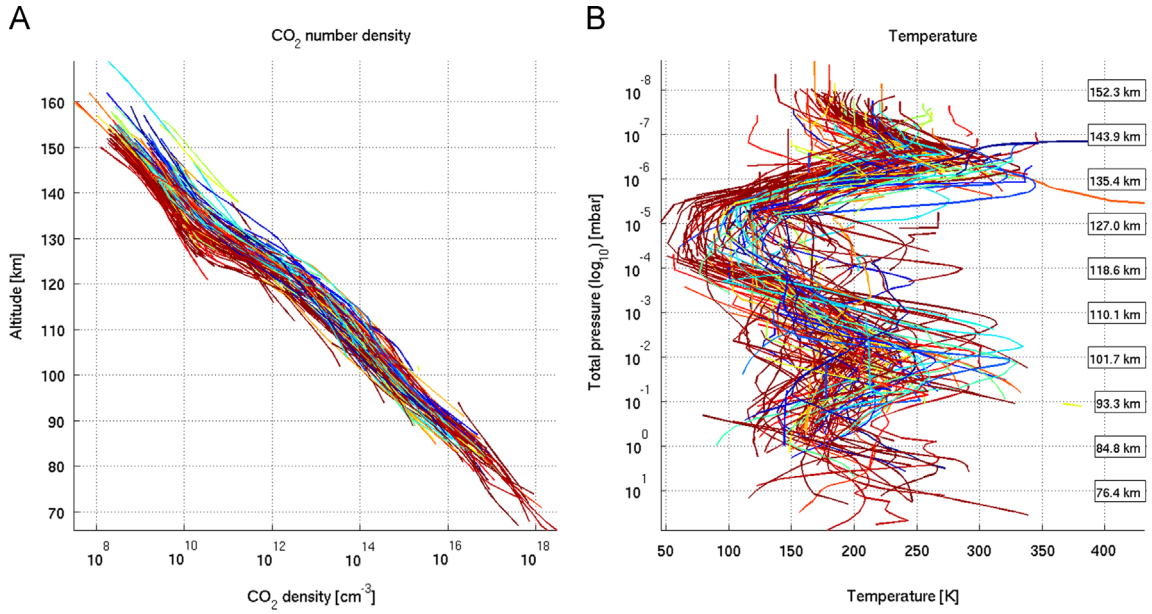

Fig. 3. CO_2 number density profiles (Panel A) and temperature profiles (Panel B) of the orbits listed in Table 2. The color code is the absolute latitude. The error bars are not displayed for clarity sake. The CO_2 number density profiles are presented as a function of the altitude, whereas the temperature profiles are as a function of the total pressure. (For interpretation of the references to color in this figure legend, the reader is referred to the web version of this article.)

mean value of 171 ± 34 K. Above, a maximum temperature of 204 ± 17 K is observed at 0.01 mbar (approximately. 102 km), and a very cold layer of 125 ± 32 K at 2.5×10^{-5} mbar ($\sim$123 km) and finally a warm layer at 3.16×10^{-7} mbar ($\sim$140 km) with a temperature of 230 ± 30 K.

4.4. Local solar time dependence

We first investigate the LST variations. In the case of SOIR, the LSTs are either 6.00 AM or 6.00 PM. The mean values of all the morning and evening temperature and CO_2 density profiles have been computed and are compared in Fig. 4.

The CO_2 density profiles obtained at the morning and the evening sides of the terminator agree within their respective standard deviations, as well as the temperature profiles. However, a small difference is observed in the CO_2 number density profiles (see Panel A of Fig. 4): above 135 km, the morning profile is higher than the evening one, by a factor smaller than 10%; in the 120 to 135 km region, the opposite is observed, with a factor up to -30%; below 115 km, the factor between AM to PM number density profiles varies between -20 and 5%. These variations are smaller than the standard deviations.

Focusing on the temperature profiles, altitudes (or pressure levels) of the minimum and maximum are equal for the 0.4 and 10^{-2} mbar levels (88 and 100 km). The temperature profiles are nearly equal at 88 km and at lower altitude. However, the temperature reached at the first maximum at 10^{-2} mbar is different for morning and evening observations. Indeed, the temperature maximum is lower by 23 K on the evening side than at the morning side. Piccialli et al. (2015) found similar temperature differences between the SPICAV–UV/VEx morning and evening observations at similar altitudes. This difference was also observed by Venera 15

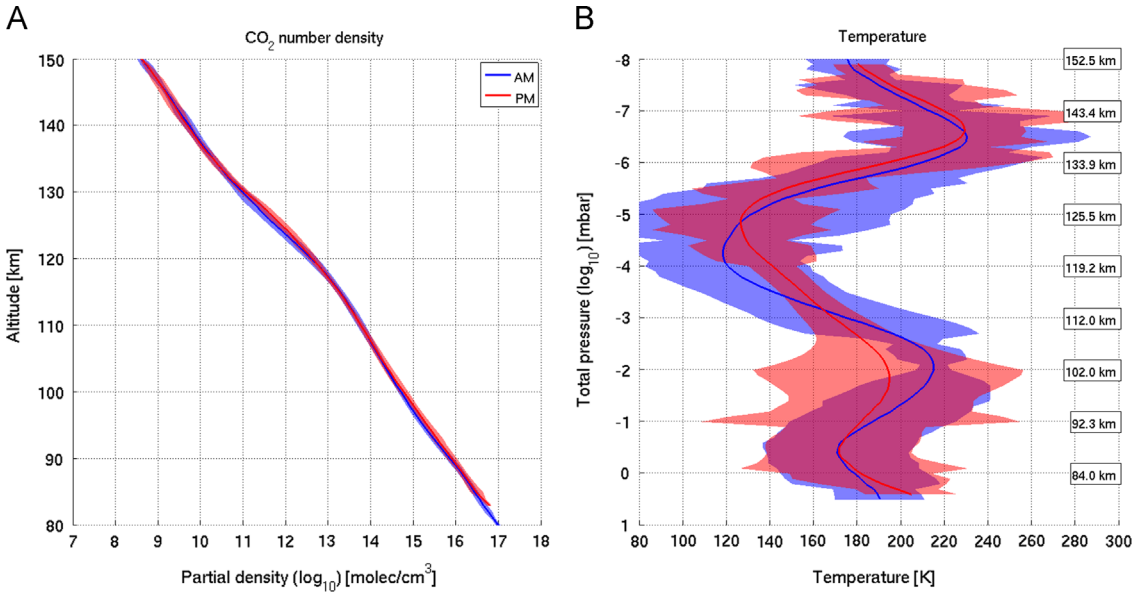

Fig. 4. Comparison between the mean morning profiles (light blue) and the mean evening side profiles (red). The CO_2 number density profiles are presented in Panel A and temperature in Panel B. The mean values are calculated on the same altitude scale for the CO_2 number density profiles, whereas calculated on the same pressure scale for temperature. In Panel B, the approximate altitude scale is also given. The standard deviations are given by the color shaded areas. (For interpretation of the references to color in this figure legend, the reader is referred to the web version of this article.)

at altitudes near 95 km (Zasova et al., 2007), indicating that at those altitudes the atmosphere was cooling during the daytime. The standard deviation of the temperature profiles are lower at these pressure levels: 12 K for AM and 20 K for PM. Above 100 km, the 2.5×10^{-5} mbar (~123 km) PM temperature minimum is located at a 6 km higher altitude (or at lower pressure levels) than the AM minimum, and reaches temperature of the same order (PM is 126 K and AM is 119 K). The 4×10^{-7} mbar (~140 km) is also observed at slightly higher altitude in the PM profile (~3 km, AM maximum temperature is 230 K and PM is 229 K).

The differences between AM and PM temperature profiles can be explained by the different wind regimes at these altitudes: above 120 km, the subsolar to antisolar (SS–AS) circulation is predominant, while in the 90 km and 120 km a transition region is found between the SS–AS circulation and the retrograde atmosphere superrotation (Brecht, 2011): winds at the morning terminator bring air from the hot dayside while they bring cold nightside air at the evening terminator.

4.5. Latitude dependence

The latitude dependence of the profiles is further addressed in the following. As in Mahieux et al. (2012), a North–South hemisphere symmetry is postulated. The same latitude bins as in Mahieux et al. (2012) are used here, i.e. 30° wide latitude bins between the Equator and 60°, and 10° wide at higher latitudes, but differentiating for the local solar time. The statistics for each latitudinal bin is summarized in Table 3. The 0–30°, 30–60°, 70–80° and 80–90° bins contain enough profiles to be statistically relevant. The 60–70° bin contains fewer profiles, which will result in larger uncertainties in the mean profiles. If possible, new measurements until the end of the VEx mission will be performed to increase the number of CO_2 measurements in these latitude regions.

The mean CO_2 density profiles (Fig. 5, Panels A for AM and C for PM) and temperature profiles (Fig. 5, Panels B for AM and D for PM) for all latitude bins are presented for both terminator sides, together with their standard deviations. These data are also tabulated and available in the Supplementary materials.

Table 3
Statistics for each latitude bin, on each terminator side.

	Number of measurements AM	Number of measurements PM	Latitudinal density of observations AM [measurements per degree]	Latitudinal density of observations PM [measurements per degree]
0–30°	15	7	0.5	0.23
30–60°	7	10	0.23	0.33
60–70°	5	5	0.5	0.5
70–80°	8	7	0.8	0.7
80–90°	25	33	2.5	3.3
Total	60	62		

Considering the mean latitude binned CO_2 number density profiles, there is a clear latitude trend at altitudes higher than 100 km on both terminator sides: the CO_2 density is larger at the Equator than at the Poles, and gradually decreases with increasing latitude. That latitude dependence vanishes at lower altitudes, below 85 km.

All the mean temperature profiles are calculated on the same pressure scale. In Panels B and D, the altitude levels are given as an indication. Small variations are observed from latitude bin to latitude bin. However, each profile always remains within the global standard deviations. This means that the time variations are larger than the latitude variations in this database.

Since the upper and lower limits of the profiles should be considered with caution, they have been cut in these plots. It is due to the fact that, first, the number of data points available is lower at the boundaries, since all the profiles do not extend up to the maximum and minimum altitude levels of each of the mean VAST temperature profiles, resulting in a bad statistics in these regions. Second, at the top of the profiles, there is dependence for the temperature on the boundary condition, which extends down to one scale height (usually 6 km at these altitudes). For these two reasons, we have a good confidence in the VAST profiles in the 80 to 150 km region.

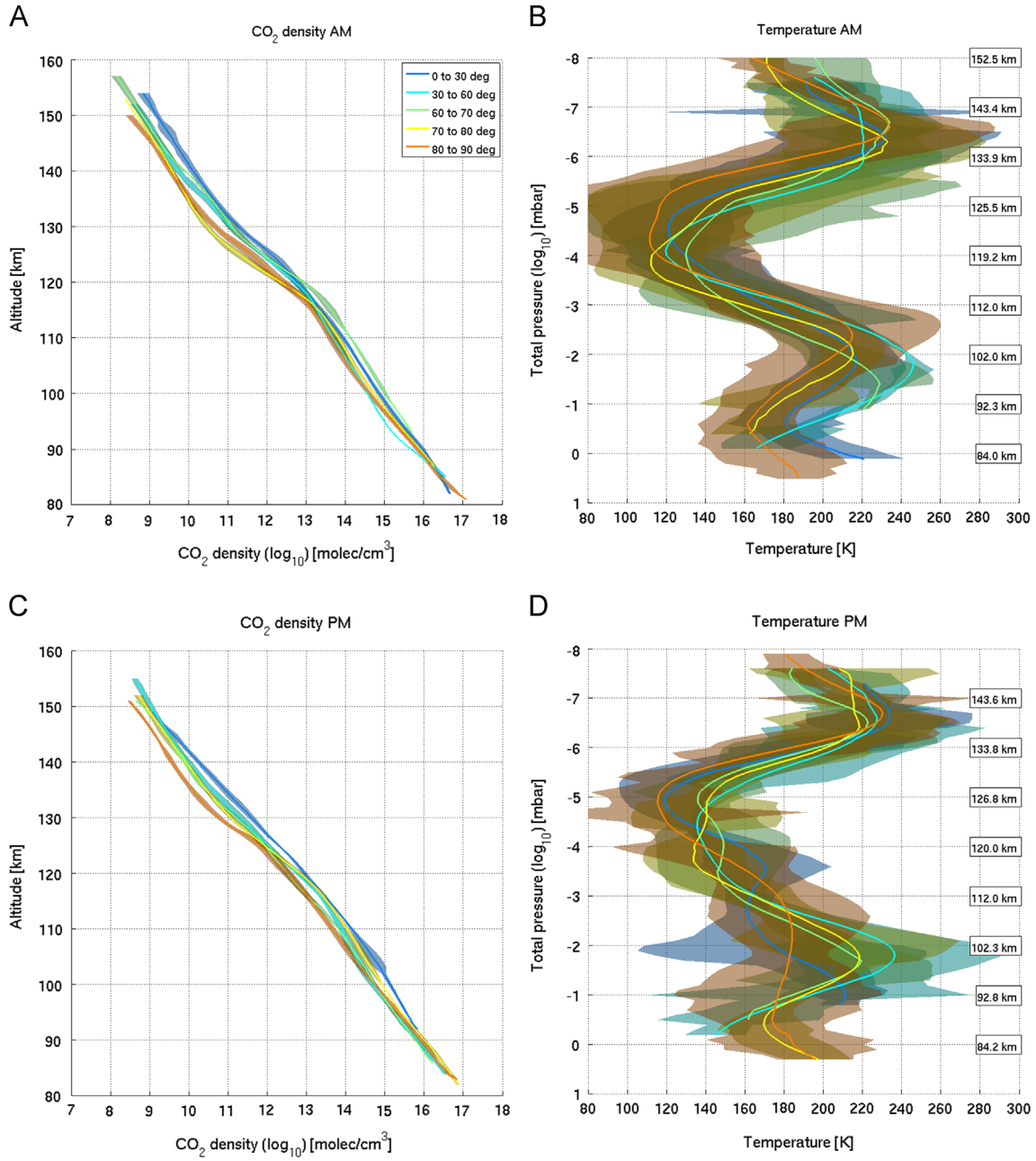

Fig. 5. Mean CO_2 number density (Panels A and C) and temperature (Panels B and D) profiles built on the latitude bins defined in Table 3, together with their standard deviation. Top Panels (A and B) are for morning measurements; bottom Panels (B and D) for evening ones. The mean values are calculated on the same altitude scale for the CO_2 number density profiles, and on the same pressure scale for temperature. In Panels B and D, the approximate altitude scale is also given.

Temperature maps have also been built on these profiles. They are presented in Fig. 6 for both terminator sides (Panel A for morning side, Panel B for evening side). A comprehensive comparison between the simulated VTGCM and measured SOIR temperature profiles, as well as a detailed description of the heat balances responsible at the terminators, is presented in the companion paper Bougher et al. (2015).

As described in this study, the wave-like structure observed in all the temperature profiles has mostly radiative explanations (Bougher et al., 2015), with probable lower contributions of atmosphere dynamical effects, such as atmospheric waves.

The warm layer at 5×10^{-7} mbar ($\sim$140 km) is observed at all latitudes, and presents small variations with latitude, with latitude binned temperatures varying between 215 and 235 K. Warm temperatures above $\sim$135 km are due to a combination of extreme ultraviolet (EUV) heating and cross terminator heat transport (advection) from the warm dayside thermosphere, e.g. Brecht and Bougher (2012). There is a good correspondence between the Venus Thermosphere General Circulation Model (VTGCM) and SOIR temperatures (Bougher et al., 2015).

The cold layer at 120–125 km is observed at all latitudes, with small differences between the morning and evening sides of the terminator. On the morning side, a maximum is observed at mid-latitudes (60–70°, $\sim$130 K), and the values decrease towards the Poles and the Equator, approaching 110 K at the Poles to 120 K at the Equator. On the evening side, a slightly warmer maximum is observed at mid-latitudes (30–80°, $\sim$140 K), and the temperature gradually decreases to the Equator ($\sim$120 K) and to the Poles ($\sim$115 K). The evening terminator side is warmer by 5 to 10 K at all latitudes than the morning side. The cold temperatures in this

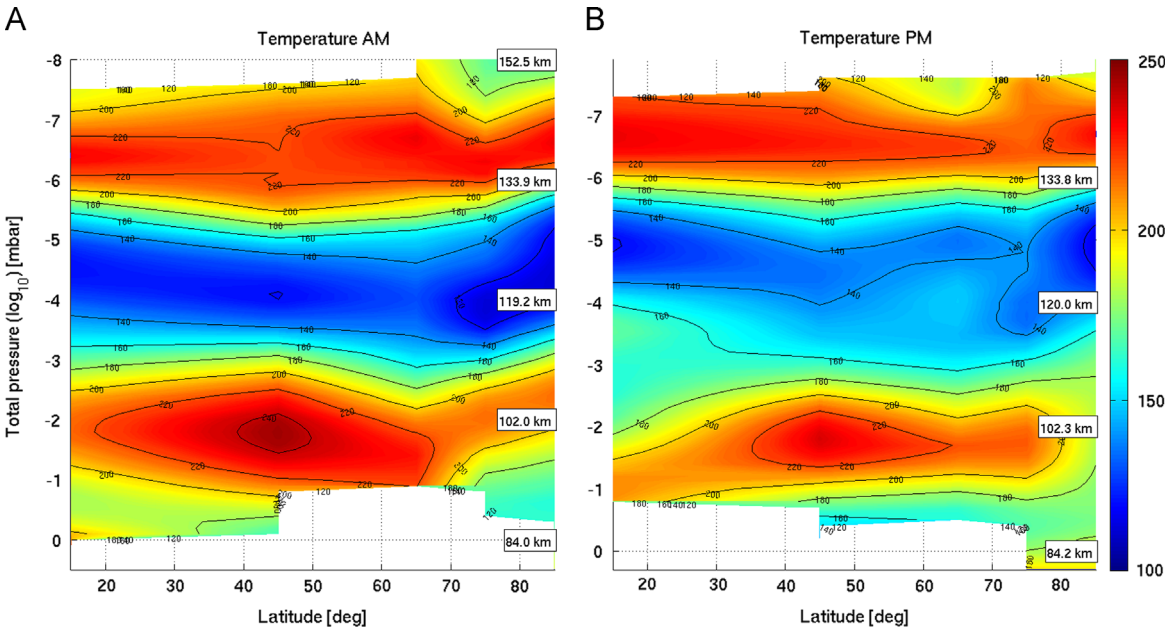

Fig. 6. Temperature maps (Panel A for morning measurements, Panel B for evening) built on the latitude binned average profiles presented in Fig. 5, covering the 1 to 10^{-8} mbar region (82 to 152 km) and all latitudes between the Equator and the Poles and considering North–South symmetry.

layer are largely due to weak NIR heating at these levels (no EUV heating), and relatively weak transport (advection from the dayside) at these latitudes along the terminators. There is reasonable correspondence between the VTGCM and SOIR temperatures, see Bougher et al. (2015).

A warm layer is observed near 100 km, with temperatures between 200 and 250 K, and is warmer on the morning side of the terminator. There is a maximum at mid-latitudes on both terminator sides, decreasing towards the Poles and the Equator. Here, the evening side is observed to be 30 K colder than the morning side of the terminator. This warm layer is largely due to transport (heat advection) from the warm dayside consistent with its strong NIR heating near this level (see Bougher et al., 2015; Brecht and Bougher, 2012). The top half of this warm layer shows a reasonable match of SOIR and VTGCM temperatures. However, below ~105 km, this secondary warm layer is missing in the VTGCM, implying that an additional heating mechanism is needed (Bougher et al., 2015; Mahieux et al., 2015a; Wilquet et al., 2012).

At the morning side of the terminator, a cold layer is observed in the 85 km region, presenting a latitudinal dependence on the morning side, decreasing from the Equator to the Poles; this dependence is not present on the evening side. This structure was already observed by Venera 15 (Zasova et al., 2007).

4.6. Comparison of the temperature profiles with other datasets

4.6.1. Equatorial region (0–30°)—Fig. 7, Panel A

Comparisons with SPICAV–UV/VEx profiles, measured on the night-side close to the terminator (Piccialli et al., 2015) are shown in Fig. 7. These profiles are single measurements, whereas the SOIR profiles are mean values calculated based on many profiles. Therefore, the SPICAV–UV profiles should be compared with the VAST standard deviation region (shaded areas). There is a good agreement between SPICAV–UV and VAST, except at the top of the SPICAV–UV profiles, where the coldest temperatures are found at higher altitudes than for SOIR. At the bottom of the profiles, the local maximum of the temperatures measured by SPICAV–UV are colder than the VAST temperatures by 20 K, and the maximum is observed at lower altitude (10 km below). Also, the slope of the SPICAV–UV temperature profiles, linked to the static stability, is different for both data sets. We explain these differences by the fact that SPICAV–UV profiles are obtained on the night side, while SOIR measures at the twilight, where the temperature profiles are a combination between day and night side structures.

VeRa/VEx profiles, provided by the VeRa team measured close to the terminator, and VAST temperature profiles are also compared in the 1 to 0.1 mbar region (~83 to 93 km). The agreement is reasonable on the whole altitude region covered by both instruments in all the latitude bins, and are in better agreement with the VAST morning profiles (in blue) than with the evening profiles (in red). VeRa temperature profiles depend on an upper boundary condition, which can be chosen between 170, 200 and 230 K. We used the profiles with a 200 K top boundary condition here. The local minimum above 0.5 mbar (~85 km) is colder in the VeRa dataset than for VAST by 10 to 15 K.

Comparisons between Clancy et al. (2012, 2003) and VAST temperatures are also presented. They show a reasonable agreement with the dayside ground-based measurements in the region between 1 and 10^{-2} mbar (83 and 103 km) on the dayside, and not with the nightside profiles. VAST is slightly warmer at lower pressure levels.

Comparisons with Pioneer Venus (PV) from Seiff et al. (1980) and Taylor et al. (1980) taken close to the terminator also show a reasonable agreement between 1 and 0.1 mbar (~83 to 93 km), with larger temperatures for VAST by 20 K. Above the inversion observed at 90 km (0.3 mbar) in Seiff et al. (1980), VAST temperatures are warmer on both sides of the terminator.

4.6.2. 30–60° Latitude region—Fig. 7, Panel B

The agreement between SPICAV–UV/VEx profiles and VAST in this latitude bin is not as good as for the Equatorial region. The slope of VAST temperature profiles in the 10^{-2} to 10^{-5} mbar (101 to 126 km) region is steeper than in the SPICAV–UV profiles. The temperatures at the top of the SPICAV–UV profiles are as cold as in VAST, but are found at an altitude higher by 20 km. The temperatures at 100 km are 60 K colder for the SPICAV–UV profiles than for VAST.

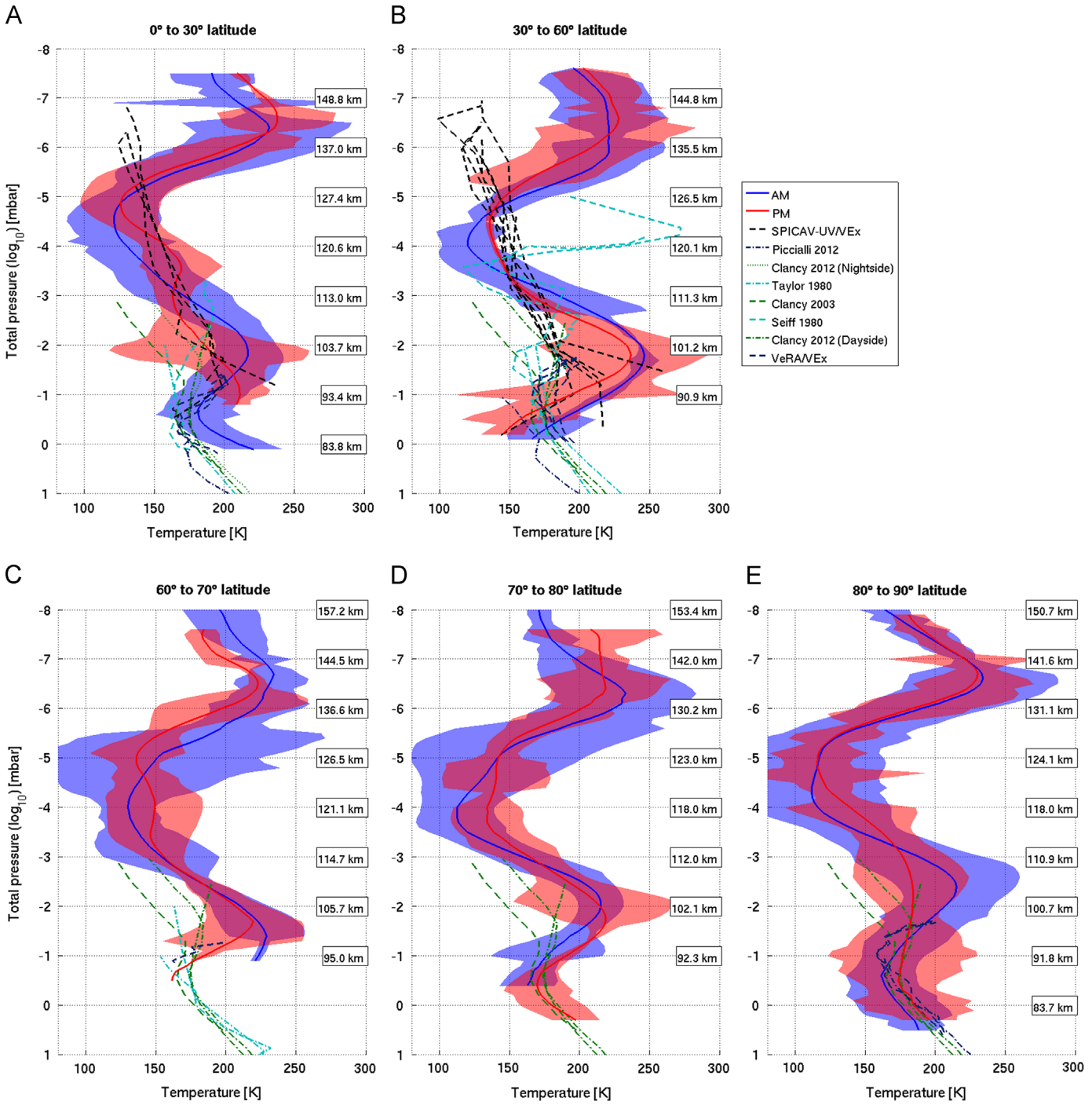

Fig. 7. Comparison of VAST temperature profiles from 4 latitude bins with literature data, for the two LST bins (AM=black, PM=red). In Panel A, the 0–30° latitude bin is considered, in Panel B the 30–60° is presented, the 60–70° latitude bin is shown in Panel C, the 70–80° region in Panel D and the 80–90° region is plotted in the Panel E. The shaded areas are the standard deviations on the SOIR temperature profiles. The altitude scale is given as an indication on the right hand side of each plot. The profiles are compares with different previously published (Clancy et al., 2012, 2003; Piccialli et al., 2012; Seiff et al., 1980; Taylor et al., 1980) and VEx temperature profiles (SPICAV-UV and VeRa). (For interpretation of the references to color in this figure legend, the reader is referred to the web version of this article.)

The nightside VeRa/VEx profile is in reasonable agreement in the 1 to 0.1 mbar (80 to 90 km) region, but the inversion seen in VAST in not observed in the VeRa profile.

The agreement with Clancy et al. (2003, 2012) is fair, the inversion seen at 1 mbar (~80 km) in VAST is observed at 0.1 mbar (~90 km) in these ground-based profiles; VAST is in better agreement with the dayside measurement than with the nightside ones. The warm layer observed in VAST at 100 km (~10^{-2} mbar) is not observed in the Clancy et al. (2012) dayside profiles.

For PV measurements from Seiff et al. (1980) and Taylor et al. (1980), the agreement is fair, but the 100 km (~10^{-2} mbar) warm layer of VAST is not observed either in these profiles.

4.6.3. 60–70° Latitude region—Fig. 7, Panel C

There is a very good agreement between the VeRa/VEx profile with the evening VAST profile at 0.1 mbar (~95 km).

The altitude overlap between PV from Seiff et al. (1980) and Taylor et al. (1980) measurements and VAST is small; the connection between PV profiles and VAST is good 0.2 mbar (~93 km).

Same conclusions as for the lower latitude bins about Clancy et al. (2003, 2012) profiles can be drawn.

4.6.4. 70–80° Latitude region—Fig. 7, Panel D

There is a very good agreement with Clancy et al. (2003, 2012) profiles below the 0.1 mbar (~92 km) pressure level. As for the other bins, the agreement is better at higher altitudes with the dayside profiles than with the nightside ones.

4.6.5. Polar region (80–90°)—Fig. 7, Panel E

VAST is compared to one VeRa/VEx temperature measurement, which is in very good agreement with the AM and PM VAST profiles. The comparison with the VeRa profile obtained from Piccialli et al. (2012) shows a good agreement within the VAST standard deviations.

The agreement with ground-based profiles from Clancy et al. (2003, 2012) is very good below 0.01 mbar (~100 km). At higher altitude, it is also very good with the dayside profile, and deviations are observed with the nightside profiles above the 0.1 mbar level (~92 km).

5. Conclusions

Based on the updated CO_2 density and temperature profiles, a new version of the Venus Atmosphere measurement from SOIR at the Terminator (VAST) compilation has been produced. The principal improvements include: (1) A newer calibration of all SOIR spectra (Vandaele et al., 2013), (2) A more complex and accurate method to consider the physical size of the slit. The observed radiance is simulated as the average of the radiances reaching the slit along 24 different LOS spanning the slit. This corrects for the bias which was seen as an altitude shift in the CO_2 number density and temperature profiles, and which was function of the latitude of the observation. (3) An improvement linked to a caveat introduced by the Bayesian Rodgers algorithm has also been implemented: only the measurements that have really been fitted are considered.

The updated VAST provides averaged CO_2 density and temperature profiles within 30° wide latitudinal bins between the Equator and 60°, and 10° wide latitudinal bins at higher latitudes, considering a North–South hemispheric symmetry. The morning–evening symmetry previously postulated (Mahieux et al., 2012) is not considered in this work anymore, since we now have enough measurements on each terminator side to differentiate between morning and evening profiles. The upper warm layer at 150 km shows small variations. We show that the latitude dependence of the cold layers is a function of the terminator side. It is not the case for the lower warm layer at 100 km, except in the polar region, where colder temperatures are observed on the evening side. The time variations of the temperature profiles are larger than the latitude variations, whereas it is not the case for the CO_2 number density profiles. Comparisons with the VTGCM (Bougher et al., 2015) show a relatively good agreement, and point out missing heating terms below 100 km.

Finally, we compare our latitude binned results to other published observations and other VEx instruments temperature profiles, and show the good agreement with most of the measurements. However, in the 100 to 150 km region, we see that the SOIR VAST profiles present a much more complicated structure than the night side profiles, which is probably a combination of the day and evening structures of the Venus temperature profiles.

Acknowledgements

Venus Express is a planetary mission from the European Space Agency (ESA). We wish to thank all ESA members who participated in the mission, in particular, H. Svedhem and D. Titov. We thank our collaborators at IASB-BIRA (Belgium), Latmos (France), and IKI (Russia). We thank CNES, CNRS, Roskosmos, and the Russian Academy of Science. The research program was supported by the Belgian Federal Science Policy Office and the European Space Agency (ESA, PRODEX program, contracts C 90268, 90113, and 17645). We acknowledge the support of the "Interuniversity Attraction Poles" program financed by the Belgian government (Planet TOPERS). The main author was supported by a grant from the Belgian American Education Foundation (BAEF), and thanks the FNRS for the position of "chargé de recherche". The research leading to these results has received funding from the European Union Seventh Framework Program (FP7/2007–2013) under grant agreement no. 606798. The authors acknowledge the support provided by ISSI, through the organization of the International Team "Towards a self-consistent model of the thermal structure of the Venus atmosphere" (http://www.issibern.ch/teams/venusatmos/). A. Piccialli acknowledges funding from the European Union Seventh Framework Program (FP7/2007-2013) under grant agreement no. 246556. The authors would like to thank Dr. T. Clancy and Dr. B. Sandor from the University of Boulder, Colorado, for their fruitful discussions and advices concerning the improvements to be made to the retrieval method.

Appendix A. Supporting information

Supplementary data associated with this article can be found in the online version at http://dx.doi.org/10.1016/j.pss.2015.02.002.

References

Banks, P.M., Kockarts, G., 1973. Aeronomy Part B. Academic Press, New York, NY.

Belyaev, D., Montmessin, F., Bertaux, J.L., Mahieux, A., Fedorova, A., Korablev, O., Marcq, E., Yung, Y., Zhang, X., 2012. Vertical profiling of SO_2 and SO above Venus' clouds by SPICAV/SOIR solar occultations. Icarus 217, 740–751.

Bertaux, J.L., Vandaele, A.C., Korablev, O., Villard, E., Fedorova, A., Fussen, D., Quémerais, E., Belyaev, D., Mahieux, A., Montmessin, F., Müller, C., Neefs, E., Nevejans, D., Wilquet, V., Dubois, J.P., Hauchecorne, A., Stepanov, A., Vinogradov, I., Rodin, A., Team, a.t.S., 2007. A warm layer in Venus' cryosphere and high altitude measurements of HF, HCl, H_2O and HDO. Nature 450, 646–649 (doi:610.1038/nature05974).

Bougher, S.W., Brecht, A., Schulte, R., Fischer, J., Parkinson, C., Mahieux, A., Wilquet, V., Vandaele, A.C., 2015. Upper atmosphere temperature structure at the Venusian terminators: a comparison of SOIR and VTGCM results. Planet. Space Sci. 113–114, 337–347.

Brecht, A., 2011. Tracing the Dynamics in Venus' Upper Atmosphere, Atmospheric and Space Sciences. University of Michigan.

Brecht, A.S., Bougher, S.W., 2012. Dayside thermal structure of Venus' upper atmosphere characterized by a global model. J. Geophys. Res. 117, E08002. http://dx.doi.org/10.1029/2012JE004079.

Clancy, R.T., Sandor, B., Moriarty-Schieven, G., 2008. Venus upper atmospheric CO, temperature, and winds across the afternoon/evening terminator from June 2007 JCMT sub-millimeter line observations. Planet. Space Sci. 56, 1344–1354.

Clancy, R.T., Sandor, B., Moriarty-Schieven, G., 2012. Thermal structure and CO distribution for the Venus mesosphere/lower thermosphere: 2001–2009 inferior conjunction sub-millimeter CO absorption line observations. Icarus 217, 779–793.

Clancy, R.T., Sandor, B.J., Moriarty-Schieven, G., 2003. Observational definition of the Venus mesopause: vertical structure, diurnal variation, and temporal instability. Icarus 161, 1–16.

Fedorova, A., Korablev, O., Vandaele, A.C., Bertaux, J.L., Belyaev, D., Mahieux, A., Neefs, E., Wilquet, V., Drummond, R., Montmessin, F., Villard, E., 2008. HDO and H_2O vertical distributions and isotopic ratio in the Venus mesosphere by solar occultation at infrared spectrometer onboard Venus Express. J. Geophys. Res., 113. http://dx.doi.org/10.1029/2008JE003146.

Grassi, D., Migliorini, A., Montabone, L., Lebonnois, S., Cardesìn-Moinelo, A., Piccioni, G., Drossart, P., Zasova, L.V., 2010. Thermal structure of Venusian nighttime mesosphere as observed by VIRTIS-Venus Express. J. Geophys. Res. 115, http://dx.doi.org/10.1029/2009JE003553.

Hedin, A.E., Niemann, H.B., Kasprzak, W.T., 1983. Global empirical model of the Venus thermosphere. J. Geophys. Res. 88, 73–83.

Mahieux, A., Berkenbosch, S., Clairquin, R., Fussen, D., Mateshvili, N., Neefs, E., Nevejans, D., Ristic, B., Vandaele, A.C., Wilquet, V., Belyaev, D., Fedorova, A., Korablev, O., Villard, E., Montmessin, F., Bertaux, J.L., 2008. In-flight performance and calibration of SPICAV/SOIR on-board Venus Express. Appl. Opt. 47, 2252–2265.

Mahieux, A., Vandaele, A.C., Drummond, R., Robert, S., Wilquet, V., Fedorova, A., Bertaux, J.L., 2010. Densities and temperatures in the Venus mesosphere and lower thermosphere retrieved from SOIR onboard Venus Express: retrieval technique. J. Geophys. Res. 115, http://dx.doi.org/10.1029/2010JE003589.

Mahieux, A., Vandaele, A.C., Robert, S., Wilquet, V., Drummond, R., Belyaev, D., Bertaux, J.L., 2015a. Venus mesospheric sulfur dioxide measurement retrieved from SOIR on board Venus Express. Planet. Space Sci. 113–114, 193–204.

Mahieux, A., Vandaele, A.C., Robert, S., Wilquet, V., Drummond, R., Lopez-Valverde, M.A., Lopez-Puertas, M., Funke, B., Bertaux, J.L., 2015b. Rotational temperatures of Venus upper atmosphere as measured by SOIR on board Venus Express. Planet. Space Sci. 113–114, 348–359.

Mahieux, A., Vandaele, A.C., Robert, S., Wilquet, V., Drummond, R., Montmessin, F., Bertaux, J.L., 2012. Densities and temperatures in the Venus mesosphere and lower thermosphere retrieved from SOIR on board Venus Express: carbon dioxide measurements at the Venus terminator. J. Geophys. Res., 117. http://dx.doi.org/10.1029/2012JE004058.

Mahieux, A., Wilquet, V., Drummond, R., Belyaev, D., Fedorova, A., Vandaele, A.C., 2009. A new method for determining the transfer function of an acousto optical tunable filter. Opt. Express 17, 2005–2014.

Migliorini, A., Grassi, D., Montabone, L., Lebonnois, S., Drossart, P., Piccioni, G., 2012. Investigation of air temperature on the nightside of Venus derived from VIRTIS-H on board Venus-Express. Icarus 217, 640–647.

Nevejans, D., Neefs, E., Van Ransbeeck, E., Berkenbosch, S., Clairquin, R., De Vos, L., Moelans, W., Glorieux, S., Baeke, A., Korablev, O., Vinogradov, I., Kalinnikov, Y., Bach, B., Dubois, J.P., Villard, E., 2006. Compact high-resolution space-borne echelle grating spectrometer with AOTF based on order sorting for the infrared domain from 2.2 to 4.3 μm. Appl. Opt. 45, 5191–5206.

Piccialli, A., Montmessin, F., Belyaev, D., Mahieux, A., Fedorova, A., Marcq, E., Bertaux, J.L., Vandaele, A.C., Korablev, O., 2015. Thermal structure of Venus upper aymosphere measured by stellar occultations with SPICAV/Venus Express. Planet. Space Sci. 113–114, 322–336.

Piccialli, A., Tellmann, S., Titov, D., Limaye, S.S., Khatuntsev, I.V., Pätzold, M., Häusler, B., 2012. Dynamical properties of the Venus mesosphere from the radio-occultation experiment VeRa onboard Venus Express. Icarus 217, 669–681.

Rodgers, C.D., 2000. Inverse Methods for Atmospheric Sounding: Theory and Practice. University of Oxford.

Seiff, A., Kirk, D.B., Young, R.E., Blanchard, R.C., Findlay, J.T., Kelly, G.M., Sommer, S.C., 1980. Measurements of thermal structure and thermal contrasts in the atmosphere of Venus and related dynamical observations: results from the four Pioneer Venus probes. J. Geophys. Res. 85, 7903–7933.

Sonnabend, G., Krötz, P., Schmülling, F., Kostiuk, T., Goldstein, J., Sornig, M., Stupar, D., Livengood, T., Hewagama, T., Fast, K., Mahieux, A., 2012. Thermospheric/mesospheric temperatures on Venus: results from ground-based high-resolution spectroscopy of CO_2 in 1990/1991 and comparison to results from 2009 and between other techniques. Icarus 217, 856–862.

Stewart, R.W., 1968. Interpretation of Mariner 5 Venera 4 data on the upper atmosphere of Venus. J. Atmos. Sci. 25, 578–579.

Svedhem, H., 2014. First Results from Venus Express Aerobraking Campaign. COSPAR, Moscow, Russia.

Taylor, F.W., Beer, R., Chahine, M.T., Diner, D.J., Elson, L.S., Haskins, R.D., McCleese, D.J., Martonchik, J.V., Reichley, P.E., Bradley, S.P., Delderfield, J., Schofield, J.T., Farmer, C.B., Froidevaux, L., Leung, J., Coffey, M.T., Gille, J.C., 1980. Structure and meteorology of the middle atmosphere of Venus: infrared remote sensing from the Pioneer Orbiter. J. Geophys. Res. 85, 7963–8006.

Tellmann, S., Häusler, B., Hinson, D.P., Tyler, G.L., Andert, T.P., Bird, M.K., Imamura, T., Pätzold, M., Remus, S., 2012. Small-scale temperature fluctuations seen by the VeRa Radio Science Experiment on Venus Express. Icarus 221, 471–480.

Tellmann, S., Pätzold, M., Häusler, B., Bird, M.K., Tyler, G.L., 2009. Structure of the Venus neutral atmosphere as observed by the Radio Science experiment VeRa on Venus Express. J. Geophys. Res., 114.

Vandaele, A.C., De Mazière, M., Drummond, R., Mahieux, A., Neefs, E., Wilquet, V., Korablev, O., Fedorova, A., Belyaev, D., Montmessin, F., Bertaux, J.L., 2008. Composition of the Venus mesosphere measured by SOIR on board Venus Express. J. Geophys. Res., 113. http://dx.doi.org/10.1029/2008JE003140.

Vandaele, A.C., Mahieux, A., Robert, S., Berkenbosch, S., Clairquin, R., Drummond, R., Letocart, V., Neefs, E., Ristic, B., Wilquet, V., Colomer, F., Belyaev, D., Bertaux, J.L., 2013. Improved calibration of SOIR/Venus Express spectra. Opt. Express 21, 21148.

Vandaele, A.C., Mahieux, A., Robert, S., Drummond, R., Wilquet, V., Bertaux, J.L., 2015. Carbon monoxide short term variability observed on Venus with SOIR/VEX. Planet. Space Sci. 113–114, 238–256.

von Zahn, U., Fricke, K.H., Hunten, D.M., Krankowsky, D., Mauersberger, K., Nier, A.O., 1980. The upper atmosphere of Venus during morning conditions. J. Geophys. Res. 85, 7829–7840.

Wilquet, V., Drummond, R., Mahieux, A., Robert, S., Vandaele, A.C., Bertaux, J.L., 2012. Optical extinction due to aerosols in the upper haze of Venus: four years of SOIR/VEX observations from 2006 to 2010. Icarus 217, 875–881.

Wilquet, V., Fedorova, A., Montmessin, F., Drummond, R., Mahieux, A., Vandaele, A.C., Villard, E., Korablev, O., Bertaux, J.L., 2009. Preliminary characterization of the upper haze by SPICAV/SOIR solar occultation in UV to mid-IR onboard Venus Express. J. Geophys. Res., 114. http://dx.doi.org/10.1029/2008JE003186.

Zasova, L.V., Ignatiev, N., Khatuntsev, I., Linkin, V., 2007. Structure of the Venus atmosphere. Planet. Space Sci. 55, 1712–1728.

Zasova, L.V., Moroz, V.I., Linkin, V.M., 1996. Venera-15, 16 and VEGA mission results as sources for improvements of the Venus reference atmosphere. Adv. Space Res. 17, 171–180.